

Anomalous Hall effect and electronic correlation in a spin-reoriented kagome antiferromagnet $LuFe_6Sn_6$

Meng Lyu(吕孟), Yang Liu(刘洋), Shen Zhang(张伸), Junyan Liu(刘俊艳), Jinying Yang(杨金颖), Yibo Wang(王一博), Yiting Feng(冯乙婷), Xuebin Dong(董学斌), Binbin Wang(王彬彬), Hongxiang Wei(魏红祥), and Enke Liu(刘恩克)

Citation: Chin. Phys. B, 2024, 33 (**10**): 107507. DOI: 10.1088/1674-1056/ad6f93
Journal homepage: http://cpb.iphy.ac.cn; http://iopscience.iop.org/cpb

What follows is a list of articles you may be interested in

Evolution of anomalous Hall effect in ferromagnetic Weyl semimetal $Nb_xZr_{1-x}Co_2Sn$

Bo-Wen Chen(陈博文) and Bing Shen(沈冰)
Chin. Phys. B, 2024, 33 (**8**): 087501. DOI: 10.1088/1674-1056/ad4a3b

Tailoring-compensated ferrimagnetic state and anomalous Hall effect in quaternary Mn-Ru-V-Ga Heusler compounds

Jin-Jing Liang(梁瑾静), Xue-Kui Xi(郗学奎), Wen-Hong Wang(王文洪), and Yong-Chang Lau(刘永昌)
Chin. Phys. B, 2024, 33 (**7**): 077504. DOI: 10.1088/1674-1056/ad34c8

Crystal growth, magnetic and electrical transport properties of the kagome magnet RCr_6Ge_6 (R=Gd-Tm)

Xingyu Yang(杨星宇), Qingqi Zeng(曾庆祺), Miao He(何苗), Xitong Xu(许锡童), Haifeng Du(杜海峰), and Zhe Qu(屈哲)
Chin. Phys. B, 2024, 33 (**7**): 077501. DOI: 10.1088/1674-1056/ad3dcf

Enhanced anomalous Hall effect in kagome magnet $YbMn_6Sn_6$ with intermediate-valence ytterbium

Longfei Li(李龙飞), Shengwei Chi(迟晟玮), Wenlong Ma(马文龙), Kaizhen Guo(郭凯臻), Gang Xu(徐刚), and Shuang Jia(贾爽)
Chin. Phys. B, 2024, 33 (**5**): 057501. DOI: 10.1088/1674-1056/ad322d

Spin reorientation in easy-plane kagome ferromagnet $Li_9Cr_3(P_2O_7)_3(PO_4)_2$

Yuanhao Dong(董元浩), Ying Fu(付盈), Yixuan Liu(刘以轩), Zhanyang Hao(郝占阳), Le Wang(王乐), Cai Liu(刘才), Ke Deng(邓可), and Jiawei Mei(梅佳伟)
Chin. Phys. B, 2023, 32 (**5**): 057506. DOI: 10.1088/1674-1056/acc2b3

SPECIAL TOPIC — Recent progress on kagome metals and superconductors

Anomalous Hall effect and electronic correlation in a spin-reoriented kagome antiferromagnet $LuFe_6Sn_6$

Meng Lyu(吕孟)[1], Yang Liu(刘洋)[1,2], Shen Zhang(张伸)[1,3], Junyan Liu(刘俊艳)[1], Jinying Yang(杨金颖)[1,2], Yibo Wang(王一博)[1,2], Yiting Feng(冯乙婷)[1,2], Xuebin Dong(董学斌)[1,2], Binbin Wang(王彬彬)[1], Hongxiang Wei(魏红祥)[1], and Enke Liu(刘恩克)[1,2,†]

[1] *Beijing National Laboratory for Condensed Matter Physics, Institute of Physics, Chinese Academy of Sciences, Beijing* 100190, *China*
[2] *University of Chinese Academy of Sciences, Beijing* 100049, *China*
[3] *Ningbo Institute of Materials Technology & Engineering, Chinese Academy of Sciences, Ningbo* 315201, *China*

(Received 11 July 2024; revised manuscript received 6 August 2024; accepted manuscript online 15 August 2024)

The kagome lattice system has been identified as a fertile ground for the emergence of a number of new quantum states, including superconductivity, quantum spin liquids, and topological electronic states. This has attracted significant interest within the field of condensed matter physics. Here, we present the observation of an anomalous Hall effect in an iron-based kagome antiferromagnet $LuFe_6Sn_6$, which implies a non-zero Berry curvature in this compound. By means of extensive magnetic measurements, a high Neel temperature, $T_N = 552$ K, and a spin reorientation behavior were identified and a simple temperature-field phase diagram was constructed. Furthermore, this compound was found to exhibit a large Sommerfeld coefficient of $\gamma = 87$ mJ·mol^{-1}·K^{-2}, suggesting the presence of a strong electronic correlation effect. Our research indicates that $LuFe_6Sn_6$ is an intriguing compound that may exhibit magnetism, strong correlation, and topological states.

Keywords: kagome lattice, anomalous Hall effect, magnetism, electronic correlation

PACS: 75.50.Ee, 72.15.–v, 75.47.–m **DOI:** 10.1088/1674-1056/ad6f93

1. Introduction

Kagome lattice materials have been extensively studied in recent years for their feature of natural triangular geometry frustration, which gives rise to a wealth of intriguing phenomena,[1–3] such as unconventional superconductivity, quantum criticality, and quantum spin liquid behavior. In terms of electronic band structure, the kagome lattice could host flat bands, Van Hove singularities, and Dirac points.[4] This makes the kagome lattice a good platform for investigating strong correlation, charge density wave (CDW), and topological electronic states.[5–7] For an antiferromagnetic (AFM) system, the geometry frustration is relatively more significant, as in the heavy fermion CePdAl,[8] the strong frustration competes with the Kondo effect, leading to an exotic quantum critical phase. In addition, both the strong correlation and the Weyl fermion state have been recognized in the AFM kagome lattices Mn_3Sn[9,10] and Mn_3Ge,[11,12] which exhibit prominent anomalous Hall effect (AHE) and anomalous Nernst effect (ANE). Compared to ferromagnets, the much lower magnetization and inherent stray fields of AFM materials with large AHE and ANE are more promising for applications. Therefore, the search for new kagome AFM materials is an interesting topic.

The RFe_6Sn_6 (R = rare earth elements) is a family of materials that exhibit high AFM order at temperatures exceeding 500 K and employ a hexagonal structure.[13] The Fe atoms in the hexagonal layer form a kagome plane. Previous Mössbauer spectroscopy, neutron diffraction, and magnetization experiments have revealed a magnetic frustration between the ferromagnetic (FM) intraplanar exchange interaction in the *ab*-plane and AFM interplanar exchange interaction along the *c*-axis in this family.[13–15] However, there is no report on the analysis of the single crystal, not even on the basic transport properties. Our recent work on the $Y_{0.5}Fe_3Sn_3$ single crystal shows that it crystallizes into a structure of the YCo_6Ge_6-type and exhibits an intriguing AHE.[16] More detailed work on single crystals is needed to further understand the physics of this family.

Here we focus on the single crystal of $LuFe_6Sn_6$. In contrast to $Y_{0.5}Fe_3Sn_3$, which adopts a YCo_6Ge_6-type structure, $LuFe_6Sn_6$ exhibits a distinctive $HfFe_6Ge_6$-type structure, a common structure observed in the 166 systems,[17,18] as exemplified by $TbMn_6Sn_6$.[19] The magnetic measurements indicate that the material is AFM ordered at $T_N = 552$ K, and exhibits a spin reorientation around 54 K. Furthermore, a weak FM state at low temperature, driven by spin reorientation, is evident. Subsequently, the specific heat measurement shows a large Sommerfeld coefficient of $\gamma = 87$ mJ·mol^{-1}·K^{-2}, indicative of a strong correlation effect. Ultimately, the AHE is observed below 140 K, elucidating a net Berry curvature in

†Corresponding author. E-mail: ekliu@iphy.ac.cn

© 2024 Chinese Physical Society and IOP Publishing Ltd

this kagome antiferromagnet.

2. Experimental details

Single crystals of $LuFe_6Sn_6$ were grown by a self-flux method using molten Sn as a solvent. High purity lutetium pieces, iron pieces and tin balls were loaded into an alumina crucible with a molar ratio of 1:6:20, which was further sealed in an evacuated quartz tube. The loaded quartz tube was heated to 1150 °C in 10 hours and held at this temperature for 4 hours to ensure sufficient melting. It was then cooled to 500 °C in 7 days. Hexagonal prismatic single crystals (inset of Fig. 1(d)) were obtained after removing excess Sn by centrifugation at 500 °C. Traces of residual Sn on the surface of the obtained crystals were mechanically removed with a blade.

The chemical composition of the obtained crystals was determined by energy dispersive x-ray (EDX) spectroscopy using a Hitachi S-4800 scanning electron microscope. To further confirm the crystal structure and lattice parameters, the as-grown single crystals were also ground to fine powder and subjected to powder x-ray diffraction (XRD) for refinement. Crystal orientation was measured using a Bruker D2 Venture diffractometer.

DC magnetic susceptibility and magnetization measurements were carried out in a magnetic property measurement system (MPMS, Quantum Design, 2–300 K). High temperature magnetic susceptibility was measured using the vibrating sample magnetometer oven in the physical property measurement system (PPMS, Quantum Design). Specific heat measurements were carried out using a thermal relaxation method in the PPMS. Electrical transport measurement, including longitudinal resistivity and Hall effect, was also carried out in the PPMS using the standard 4-wire method. The magnetoresistance and Hall effect measurements were carried out by scanning both negative and positive magnetic fields to eliminate errors from the lead contacts.

3. Experimental results and discussion

$LuFe_6Sn_6$ crystallizes into a layered hexagonal $HfFe_6Ge_6$-type structure (Fig. 1(a)), with space group $P6/mmm$. The Fe atoms form a kagome layer as shown in Fig. 1(b). It has been reported that under ideal conditions the Fe atoms exhibit an easy FM plane and an AFM interaction along the c-axis, as indicated by the red arrows in Fig. 1(a). Nevertheless, 30% of the Fe moments deviate from the c-axis in the actual crystals as a consequence of the under stoichiometry of the Lu atoms.[13] Our EDX measurements on single crystals also indicate a significant deficiency of Lu atoms, resulting in an under-stoichiometric chemical formula of $Lu_{0.8}Fe_6Sn_{6.2}$. This is in close agreement with the reported polycrystalline composition.[13–15] Figure 1(c) shows the powder x-ray diffraction pattern of $LuFe_6Sn_6$, which agrees well with the calculated pattern based on the refined crystal structure, giving lattice parameters of $a = 5.349$ Å, $c = 8.876$ Å. The single crystal XRD pattern displays the only Bragg peak of (l00), see Fig. 1(d), indicating that the exposed surface of the hexagonal prism (the inset of Fig. 1(d)) is the ac-plane. The long axis of the crystals can be determined as the c-axis.

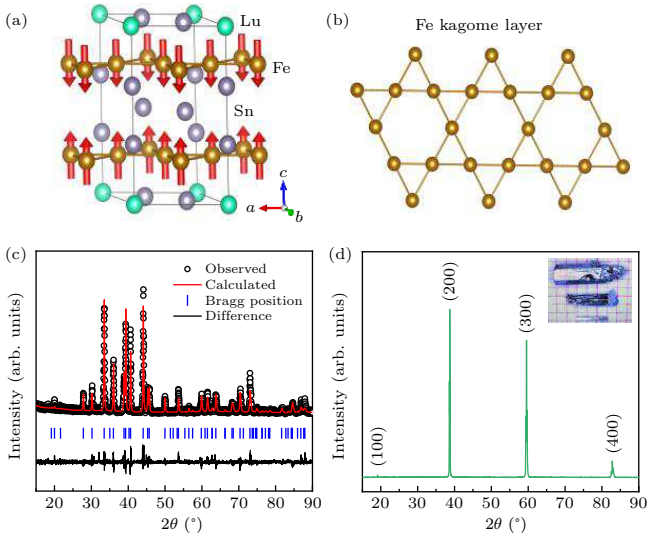


Fig. 1. (a) Crystal structure of $LuFe_6Sn_6$. The arrowed layers represent the Fe kagome plane, which is indicative of the FM interaction in the ab-plane and the AFM interaction along the c-axis. (b) The amplified Fe kagome layer. (c) Powder XRD pattern, compared with the calculated pattern based on the refined crystal structure. (d) The single crystal XRD pattern of the exposed surface of the single crystals in the inset corresponding to the (l00) plane.

The high-temperature magnetic susceptibility $\chi_{ab}(T)$ measured between 320 K and 650 K with magnetic field applied in the ab-plane is shown in Fig. 2(a). A distinct kink characterizing the AFM ordering is observed at $T_N = 552$ K, in close proximity to the value reported in a polycrystalline sample.[15] Below T_N, χ_{ab} increases continuously with decreasing temperature. This obviously deviates from the conventional AFM system, suggesting that the magnetism in this compound is inherently unstable. Figure 2(b) shows the temperature-dependent zero-field cooled (ZFC) and field cooled (FC) $\chi_{ab}(T)$ and $\chi_c(T)$ (with $B\|c$) curves between 2 K and 300 K. A strong magnetic anisotropy is observed, with a considerable ratio of $\chi_{ab}/\chi_c = 107$ at $T = 2$ K, indicative of a tendency for spins to orient in the ab-plane at low temperatures. Upon cooling to lower temperatures from 300 K, both χ_{ab} and χ_c exhibit a sharp increase at about 54 K, indicating a spin reorientation character corresponding to a spin-flop phase below this temperature. By plotting the $\mathrm{d}\chi_{ab}/\mathrm{d}T$ curve in the inset of Fig. 2(b), a sharp minimum is observed at 24 K, which suggests that the material may exhibit FM behavior at lower temperatures. Furthermore, the spin reorientation transition can also be characterized in the $\mathrm{d}\chi_{ab}/\mathrm{d}T$ curve.

It is evident from the magnetization curves $M_{ab}(B)$ that the FM behavior is indicated by the application of a magnetic field in the ab-plane, as illustrated in Fig. 2(c). $M_{ab}(B)$ exhibits

a tendency to saturate at a field of 0.28 T, with a saturation moment of 1.47 μ_B/f.u. at $T = 2$ K. The continuous increase of the M_{ab} at higher fields suggests that this is a weak FM state, which means that the moments of the Fe could be tilted with the *ab*-plane. Meanwhile, in Fig. 2(d) we also present the magnetization curves $M_c(B)$ with the magnetic field applied along the *c*-axis. $M_c(B)$ shows a slow increase below 2 T and then a rapid increase with increasing field at low temperatures, revealing a probable metamagnetic transition. By means of detailed magnetism measurements, a simple field–temperature phase diagram is constructed with the field in the *ab*-plane below 100 K, as shown in Fig. 2(e). From this, one can immediately capture the magnetism of $LuFe_6Sn_6$.

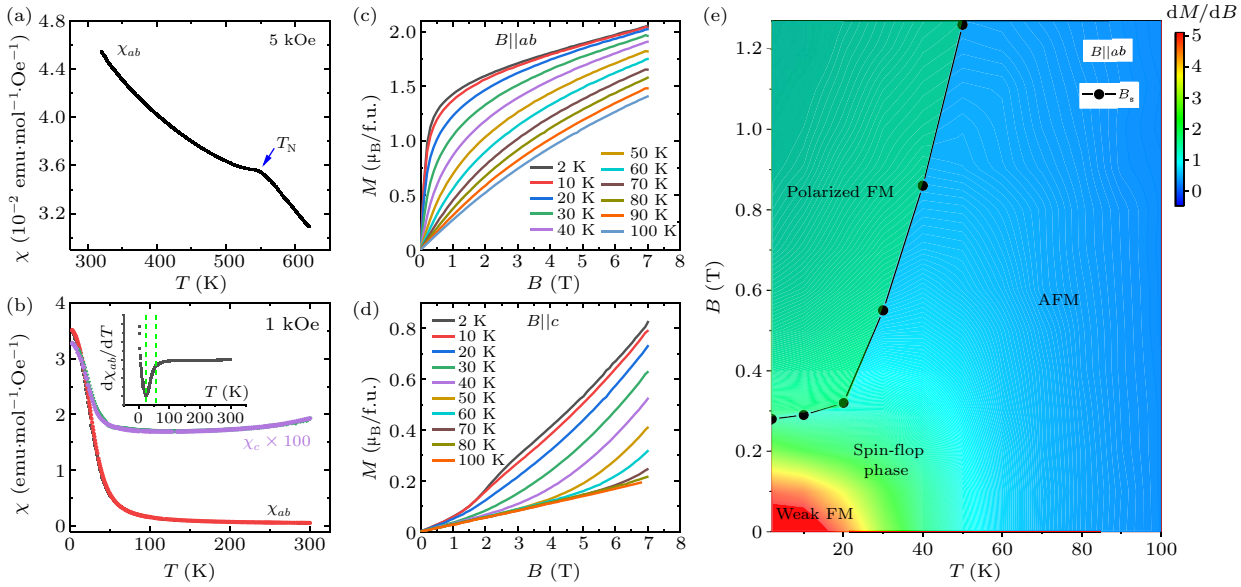


Fig. 2. (a) High temperature magnetic susceptibility of $LuFe_6Sn_6$ with $B||ab$. (b) Anisotropic ZFC and FC magnetic susceptibility between $B||ab$ and $B||c$ below room temperature. It shows that the ZFC and FC curves almost overlap in different orientations. The inset shows $d\chi_{ab}/dT$. (c) and (d) Magnetization curves below 100 K with $B||ab$ and $B||c$. (e) The T–B phase diagram with the field in the *ab* plane.

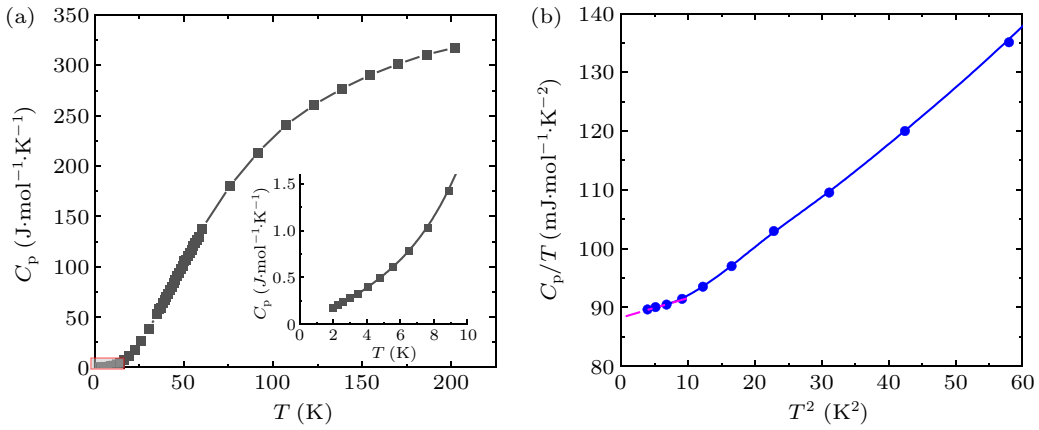


Fig. 3. (a) The specific heat as a function of temperature. The inset depicts the amplification at low temperatures. (b) C_p/T vs. T^2 for $T^2 < 60$ K. From this, the Sommerfeld coefficient can be estimated as $\gamma = 87$ mJ·mol^{-1}·K^{-2} by extrapolating the lower linear part to zero temperature.

In order to further characterize the magnetism of $LuFe_6Sn_6$, the zero-field specific heat $C_p(T)$ measurement was performed between 2 K and 200 K, as shown in Fig. 3(a). At $T = 200$ K, the specific heat is close to the Dulong–Petit limit of $3nR = 324.25$ J·mol^{-1}·K^{-1}, where n is the number of atoms per formula unit, and R is the universal gas constant (8.314 J·mol^{-1}·K^{-1}). As the temperature decreases to 2 K, there appears to be no discernible anomaly in $C_p(T)$, indicating that the spin-flop transition is thermodynamically weak in this compound. However, it is discovered that the Sommerfeld coefficient is notably high, with $\gamma = 87$ mJ·mol^{-1}·K^{-2}, estimated by extrapolating C_p/T versus T^2 to zero temperature, as shown in Fig. 3(b). The observation of a slight deviation from the linear fit at higher temperatures suggests that the FM fluctuations may serve to enhance the γ value. The large Sommerfeld coefficient is also observed in the isostructural $LuFe_6Ge_6$ and $YbFe_6Ge_6$,[20] and is comparable to that of other iron-based compounds, such as the typical iron-based superconductors[21] and the two-dimensional van der Waals ferromagnetic Fe_3GeTe_2,[22,23] suggesting the presence

of a strong electronic correlation effect in this compound. It should be noted that the Sommerfeld coefficients of other typical magnetic kagome topological materials such as $Co_3Sn_2S_2$ (10.8 mJ·mol^{-1}·K^{-2}),[24] Mn_3Ge (22.5 mJ·mol^{-1}·K^{-2}) and Mn_3Sn (32.5 mJ·mol^{-1}·K^{-2}),[25] are much lower than that of $LuFe_6Sn_6$.

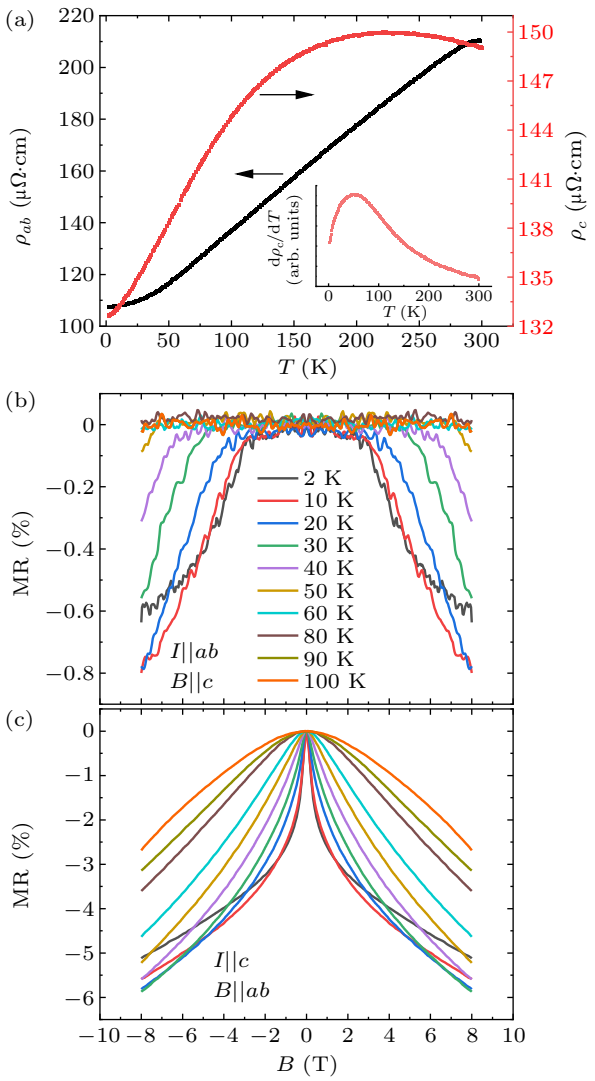


Fig. 4. (a) Anisotropic electrical resistivity between $I\|ab$ and $I\|c$. The inset shows $\mathrm{d}\rho_c/\mathrm{d}T$ curve, where the broad peak represents the spin reorientation temperature. (b) and (c) The MR with $I\|ab$, $B\|c$ and $I\|c$, $B\|ab$, respectively.

Having established the magnetic phase diagram of $LuFe_6Sn_6$, we now turn to look into its electrical transport properties. Figure 4(a) shows the temperature dependent electrical resistivity at zero field with $I\|ab$ and $I\|c$. When the current is applied in the kagome ab-plane, ρ_{ab} exhibits a normal metallic behavior, and almost linear temperature dependence above 50 K. In comparison, ρ_c shows a broad peak around 200 K, and decreases rapidly below 100 K, signaling a strongly anisotropic behavior. The differential of ρ_c behaves with a clear broad peak around 54 K, see the inset of Fig. 4(a), corresponding to the anomaly observed in the magnetic susceptibility, also indicating the spin reorientation character. Figures 4(b) and 4(c) present the field dependent magnetoresistance (MR) below 100 K with $I\|ab$, $B\|c$ and $I\|c$, $B\|ab$, respectively. The MR at $B\|c$ shows a clear transition around 2 T at 2 K, the same as it observed in the magnetization curve, revealing a metamagnetic-like behavior. The large transition of MR with the field may be related to the electronic structure. When the field is applied in the ab plane, the MR is an order of magnitude larger than it along the c-axis, again suggesting the strong anisotropic behavior. The negative MR in both directions may be related to the weak FM behavior. Although the weak FM state exists at temperatures below 24 K, the strong FM component can be clearly observed in the $M_{ab}(B)$ curves above this temperature. The behavior of the MR can be attributed to the competition between the AFM interaction along the c-axis and the FM interaction in the ab-plane.

Figure 5(a) displays the field dependent Hall resistivity $\rho_{ca}(B)$ of $LuFe_6Sn_6$ with $I\|c$, $B\|ab$. At low temperatures, ρ_{ca} tends to saturate with increasing field, which is very similar to the behavior of the magnetization curve. The comparison of $M(B)$ and $\rho_{ca}(B)$ at $T = 2$ K is shown in Fig. 5(b). In the weak FM state shown above, the saturation feature of ρ_{ca} is a typical characteristic of the anomalous Hall effect. In this scenario, the total Hall resistivity can be described by the relation $\rho_{ca} = \rho_{ca}^{\mathrm{N}} + \rho_{ca}^{\mathrm{A}} = R_0\mu_0 H + R_{\mathrm{S}}\mu_0 M$, where ρ_{ca}^{N} and ρ_{ca}^{A} denote the normal and anomalous Hall resistivity, and R_0 and R_{S} denote the normal and anomalous Hall coefficients, respectively. Figure 5(b) inset shows the fitting curves of the Hall resistivity at $T = 2$ K, from which we can determine the carrier density to be $n = 1/(eR_0) = 1.17 \times 10^{22}$ cm^{-3}. By further extrapolating $\rho_{ca}^{\mathrm{A}}(B)$ to zero field, $\rho_{ca}^{\mathrm{A}}(T)$ can be obtained.

Figure 5(c) shows the temperature dependent Hall resistivity $\rho_{ca}^{\mathrm{A}}(T)$. With increasing temperature, ρ_{yx}^{A} gradually decays and disappears above 140 K. To gain further insight into the AHE, the anomalous Hall conductivity (AHC) is calculated by $\sigma_{ac}^{\mathrm{A}} = \rho_{ca}^{\mathrm{A}}/(\rho_{ca}^{\mathrm{A}\,2} + \rho_c\rho_a)$. As shown in Fig. 5(d), σ_{ac}^{A} is 103 Ω^{-1}·cm^{-1} at $T = 2$ K. While this AHC value is one order of magnitude smaller than that observed in the typical ferromagnetic Weyl semimetal, such as $Co_3Sn_2S_2$ (1130 Ω^{-1}·cm^{-1} at 2 K),[26] it is nevertheless comparable to that observed in some antiferromagnetic topological systems, such as the kagome lattices Mn_3Sn and Mn_3Ge.[12] Given that the AHC of $LuFe_6Sn_6$ remains almost unchanged below 20 K and that the electrical conductivity (σ_{xx}) is situated within the intrinsic regime ($\sigma_{xx} \sim 3 \times 10^3$–$5 \times 10^5$ Ω^{-1}·cm^{-1}) in the unified model,[27] it seems plausible that the AHE may have its origin in the intrinsic non-zero Berry curvature. The anomalous Hall angle (AHA) is also presented in Fig. 5(d), which shows that the maximum AHA is 1.1%, a value comparable to that observed in a normal ferromagnetic material.

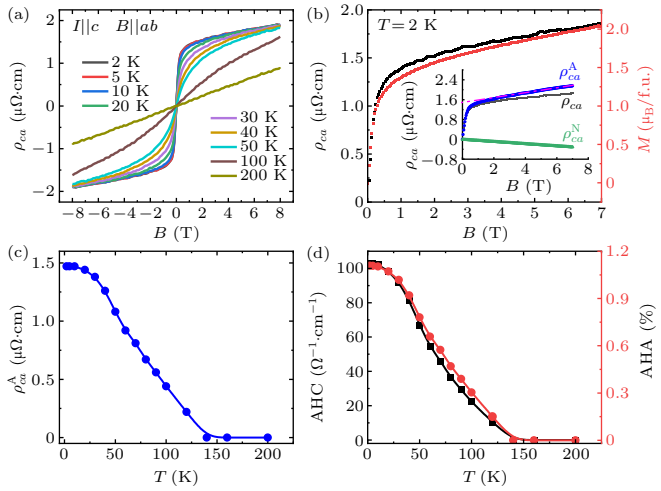


Fig. 5. (a) The Hall resistivity with $I||c$, $B||ab$, showing a typical AHE at low temperatures. (b) The comparison of $M(B)$ and $\rho_{ca}(B)$ at $T = 2$ K. The inset shows the fitted curves of the Hall resistivity by $\rho_{ca} = \rho_{ca}^{N} + \rho_{ca}^{A} = R_0\mu_0 H + R_S\mu_0 M$ at $T = 2$ K. (c) The estimated anomalous Hall resistivity as a function of temperature. (d) The calculated AHC and AHA.

In comparison with previous experiments on the polycrystalline $LuFe_6Sn_6$, our single crystal investigation has revealed a strong anisotropy of this compound. The spin reorientation behavior of RFe_6Sn_6 was also characterized by Mössbauer spectroscopy and neutron diffraction measurements before.[13–15] It has been claimed that this behavior is due to magnetically frustration driven by the under stoichiometry of the R atoms. For the single crystal of $LuFe_6Sn_6$, the Lu atom is also deficient, which appears to be a common occurrence in this system. Furthermore, the geometry frustration of the Fe-kagome lattice should also be taken into account. For example, the kagome material FeGe shows an A-type collinear AFM order at 400 K, then a CDW phase coupled with AFM order below 110 K, and finally a c-axis biconical AFM structure around 60 K.[28–30] In FeGe, the interaction between geometric frustration and the strong correlation plays an important role in these rich spin states.[30,31] The combined data from previous Mössbauer spectroscopy and our magnetic measurements indicate that the spins of the iron atoms in $LuFe_6Sn_6$ may be canted, with the spins oriented along the direction between the kagome plane and the c-axis. At low temperatures, the spins tend to align in the plane.

The strong correlation effect observed in $LuFe_6Sn_6$ is a notable feature, as it has been reported previously in the analogous compounds $LuFe_6Ge_6$ and $YbFe_6Ge_6$.[20] Given that $LuFe_6Sn_6$ and $YbFe_6Ge_6$ exhibit comparable large Sommerfeld coefficients, it can be concluded that the rare earth elements have no impact on the correlation effect. It is well established that the hopping frustration in a kagome lattice may give rise to the formation of strong correlations. This phenomenon has been observed in Ni_3In,[32] where destructive interference in the kagome plane induces flat bands. These flat bands subsequently result in a heavy fermion behavior. Another potential scenario is that 3d-electron hybridization could also give rise to a strong correlation effect, as observed in iron-based superconductors, such as AFe_2As_2 (A = K, Rb, Cs).[21]

Considering the weak FM state at low temperatures, the behavior of the AHE in $LuFe_6Sn_6$ seems to be normal. The AHE remains non-zero above the spin reorientation temperature, which can be explained by the high-field-induced FM component, as shown in the magnetization curves of Fig. 2(c). Moreover, the magnitude of the AHE in $LuFe_6Sn_6$ is even larger than that observed in the canted antiferromagnet $YbMnBi_2$ (26 Ω^{-1}·cm^{-1} at 120 K),[33] where the non-zero Berry curvature contributes to the AHE and further generates a giant ANE. The presence of non-trivial topological bands in the kagome lattice of $LuFe_6Sn_6$ is anticipated, with the intrinsic generation of a net Berry curvature that will contribute to the AHE. Further investigation of the ANE in $LuFe_6Sn_6$ is therefore warranted. Given the ambiguous nature of the magnetic structure, it is challenging to discern the detailed electronic bands and potential topological features. In order to gain further insight into the physics of $LuFe_6Sn_6$, it is anticipated that more comprehensive neutron diffraction and spectroscopy experiments on single crystals will be conducted.

4. Conclusion

In conclusion, the synthesis of the kagome single crystal $LuFe_6Sn_6$ was successfully achieved. This enables us to investigate the anisotropic low-temperature properties in the AFM state. Our findings indicate that the material exhibits a pronounced anisotropy between the kagome ab-plane and the c-axis. The construction of the phase diagram allows for the clear presentation of the weak FM state resulting from spin reorientation. Moreover, a prominent AHE was observed below 140 K, which could be attributed to the presence of non-zero Berry curvature. The specific heat measurement indicates that this material exhibits a strong correlation effect. The hopping frustration from the iron kagome plane and the hybridization between 3d electrons are the potential reasons for this phenomenon. Our study has identified a number of exotic properties exhibited by the kagome material $LuFe_6Sn_6$. Further investigation of this compound, including neutron diffraction and theoretical calculations, may reveal more insights.

Acknowledgments

Project supported by the National Key Research and Development Program of China (Grant Nos. 2022YFA1403400, 2019YFA0704900, and 2022YFA1403800), the Fundamental Science Center of the National Natural Science Foundation of China (Grant No. 52088101), the National Natural Science Foundation of China (Grant Nos. 11974394 and 12174426), the Strategic Priority Research Program (B) of the Chinese

Academy of Sciences (CAS) (Grant No. XDB33000000), the CAS Project for Young Scientists in Basic Research (Grant No. YSBR-057), the Synergetic Extreme Condition User Facility (Grant No. SECUF), and the Scientific Instrument Developing Project of CAS (Grant No. ZDKYYQ20210003).

References

[1] Yin J X, Lian B and Hasan M Z 2022 *Nature* **612** 647
[2] Coleman P and Nevidomskyy A H 2010 *J. Low Temp. Phys.* **161** 182
[3] Zhou Y, Kanoda K and Ng T K 2017 *Rev. Mod. Phys.* **89** 025003
[4] Mielke A 1991 *J. Phys. A* **24** L73
[5] Provenzano P P 2020 *Nat. Mater.* **19** 130
[6] Wang Y, Wu H, McCandless G T, Chan J Y and Ali M N 2023 *Nat. Rev. Phys.* **5** 635
[7] Wang Q, Lei H, Qi Y and Felser C 2024 *Accounts of Materials Research* **5** 786
[8] Zhao H, Zhang J, Lyu M, Bachus S, Tokiwa Y, Gegenwart P, Zhang S, Cheng J, Yang Y F, Chen G, Isikawa Y, Si Q, Steglich F and Sun P 2019 *Nat. Phys.* **15** 1261
[9] Nakatsuji S, Kiyohara N and Higo T 2015 *Nature* **527** 212
[10] Ikhlas M, Tomita T, Koretsune T, Suzuki M T, Nishio-Hamane D, Arita R, Otani Y and Nakatsuji S 2017 *Nat. Phys.* **13** 1085
[11] Nayak A K, Fischer J E, Sun Y, Yan B, Karel J, Komarek A C, Karel J, Komarek A C, Shekhar, Nitesh C, Kumar N, Schnelle W, Kübler J, Felser C and Parkin S S 2016 *Science Advances* **2** e1501870
[12] Chen T, Tomita T, Minami S, Fu M, Koretsune T, Kitatani M, Muhammad I, Nishio-Hamane D, Ishii R, Ishii F, Arita R and Nakatsuji S 2021 *Nat. Commun.* **12** 572
[13] Mazet T and Malaman B 2000 *J. Magn. Magn.c Mater.* **219** 33
[14] Rao X L and Coey J M D 1997 *J. Appl. Phys.* **81** 5181
[15] Mazet T and Malaman B 2001 *J. Alloy. Compd.* **325** 67
[16] Liu Y, Lyu M, Liu J, Zhang S, Yang J, Du Z, Wang B, Wei H and Liu E 2023 *Chin. Phys. Lett.* **40** 047102
[17] Venturini G, Chafik B, Idrissi E and Malaman B 1991 *J. Magn. Magn. Mater.* **94** 35
[18] Zhang X, Liu Z, Cui Q, Guo Q, Wang N, Shi L, Zhang H, Wang W, Dong X, Sun J, Dun Z and Cheng J 2022 *Phys. Rev. Materials* **6** 105001
[19] Yin J X, Ma W, Cochran T A, Xu X, Zhang S S, Tien H J, Shumiya N, Cheng G, Jiang K, Lian B, Song Z, Chang G, Belopolski I, Multer D, Litskevich M, Cheng Z J, Yang X P, Swidler B, Zhou H, Lin H, Neupert T, Wang Z, Yao N, Chang T R, Jia S and Zahid Hasan M 2020 *Nature* **583** 533
[20] Avila M A, Takabatake T, Takahashi Y, Bud'ko S L and Canfield P C 2005 *J. Phys.: Condens. Matter* **17** 6969
[21] Wu Y P, Zhao D, Wang A F, Wang N Z, Xiang Z J, Luo X G, Wu T and Chen X H 2016 *Phys. Rev. Lett.* **116** 147001
[22] Sun Y, Zhang J, Yao T, Sun X F, Ke S H, Zhang J and Zhou S M 2023 *Phys. Rev. B* **107** 094416
[23] Zhang Y, Lu H, Zhu X, Tan S, Feng W, Liu Q, Zhang W, Chen Q Y, Liu Y, Luo X B, Xie D H, Luo L Z, Zhang Z J and Lai X 2018 *Science Advances* **4** eaao6791
[24] Schnelle W, Leithe J A, Rosner H, Schappacher F M, Pöttgen R, Pielnhofer F and Weihrich R 2013 *Phys. Rev. B* **88** 144404
[25] Tomita T, Minami S, Ikhlas M, Nakamura H, Arita R and Nakatsuji S 2022 *J. Phys.: Conf. Series* **2164** 012065
[26] Liu E, Sun Y, Kumar N, Muechler L, Sun A, Jiao L, Yang S Y, Liu D, Liang A, Xu Q, Kroder J, Süß V, Borrmann H, Shekhar C, Wang Z, Xi C, Wang W, Schnelle W, Wirth S, Chen Y, Goennenwein S T B and Felser C 2018 *Nat. Phys.* **14** 1125
[27] Onoda S, Sugimoto N and Nagaosa N 2008 *Phys. Rev. B* **77** 165103
[28] Bernhard J, Lebech B, Beckman O 1984 *J. Phys. F: Metal Physics* **14** 2379
[29] Bernhard J, Lebech B, Beckman O 1988 *J. Phys. F: Metal Physics* **18** 539
[30] Teng X, Chen L, Ye F, Rosenberg E, Liu Z, Yin J X, Jiang Y X, Oh J S, Hasan M Z, Neubauer K J, Gao B, Xie Y, Hashimoto M, Lu D, Jozwiak C, Bostwick A, Rotenberg E, Birgeneau R J, Chu J H, Yi M and Dai P 2022 *Nature* **609** 490
[31] Chen L, Teng X, Tan H, Winn B L, Granroth G E, Ye F, Yu D H, Mole R A, Gao B, Yan B, Yi M and Dai P 2024 *Nat. Commun.* **15** 1918
[32] Ye L, Fang S, Kang M, Kaufmann J, Lee Y, John C, Neves P M, Zhao S Y F, Denlinger J, Jozwiak C, Bostwick A, Rotenberg E, Kaxiras E, Bell D C, Janson O, Comin R and Checkelsky J G 2024 *Nat. Phys.* **20** 610
[33] Pan Y, Le C, He B, Watzman S J, Yao M, Gooth J, Heremans J P, Sun Y and Felser C 2021 *Nat. Mater.* **21** 203